PCCP

PAPER

View Article Online
View Journal | View Issue

Cite this: *Phys. Chem. Chem. Phys.*, 2017, **19**, 23162

Photophysical characterization and time-resolved spectroscopy of a anthradithiophene dimer: exploring the role of conformation in singlet fission†

Jacob C. Dean,[a] Ruomeng Zhang,[a] Rawad K. Hallani,‡[b] Ryan D. Pensack,[a] Samuel N. Sanders,[c] Daniel G. Oblinsky,[a] Sean R. Parkin,[b] Luis M. Campos,[c] John E. Anthony[b] and Gregory D. Scholes*[a]

Received 5th June 2017,
Accepted 4th August 2017

DOI: 10.1039/c7cp03774k

rsc.li/pccp

Quantitative singlet fission has been observed for a variety of acene derivatives such as tetracene and pentacene, and efforts to extend the library of singlet fission compounds is of current interest. Preliminary calculations suggest anthradithiophenes exhibit significant exothermicity between the first optically-allowed singlet state, S_1, and 2 × T_1 with an energy difference of >5000 cm^{-1}. Given the fulfillment of this ingredient for singlet fission, here we investigate the singlet fission capability of a difluorinated anthradithiophene dimer (2ADT) covalently linked by a (dimethylsilyl)ethane bridge and derivatized by triisobutylsilylethynyl (TIBS) groups. Photophysical characterization of 2ADT and the single functionalized ADT monomer were carried out in toluene and acetone solution *via* absorption and fluorescence spectroscopy, and their photo-initiated dynamics were investigated with time-resolved fluorescence (TRF) and transient absorption (TA) spectroscopy. In accordance with computational predictions, two conformers of 2ADT were observed *via* fluorescence spectroscopy and were assigned to structures with the ADT cores *trans* or *cis* to one another about the covalent bridge. The two conformers exhibited markedly different excited state deactivation mechanisms, with the minor *trans* population being representative of the ADT monomer showing primarily radiative decay, while the dominant *cis* population underwent relaxation into an excimer geometry before internally converting to the ground state. The excimer formation kinetics were found to be solvent dependent, yielding time constants of ~1.75 ns in toluene, and ~600 ps in acetone. While the difference in rates elicits a role for the solvent in stabilizing the excimer structure, the rate is still decidedly long compared to most singlet fission rates of analogous dimers, suggesting that the excimer is neither a kinetic nor a thermodynamic trap, yet singlet fission was still not observed. The result highlights the sensitivity of the electronic coupling element between the singlet and correlated triplet pair states, to the dimer conformation in dictating singlet fission efficiency even when the energetic requirements are met.

Introduction

Singlet fission is the process whereby two triplet excitons are formed from one singlet exciton, with overall spin being conserved throughout the conversion. The exact mechanism and associated molecular design principles leading to efficient fission have recently been a topic of significant interest because of its potential for improving single-junction photovoltaic efficiency limitations from 34% (Shockley–Queisser limit) to 45% when used as a sensitizer in such devices.[1–3] The enhancement comes from the ability of these devices to harvest high-energy photons (well in excess of the optical bandgap) without significant losses to thermalization which typically plague photovoltaic conversion efficiency. This occurs through rapid conversion of the initial singlet excitation into two low-lying triplet excitons, which can later be converted into charges at an appropriate charge-separating interface. The fundamental requirements for singlet fission have been discussed in detail,[4–8] and can be simplified into two essential ingredients: energy conservation ($E(S_1) \geq 2E(T_1)$) and

[a] *Department of Chemistry, Princeton University, Princeton, NJ 08544, USA. E-mail: gscholes@princeton.edu*
[b] *Department of Chemistry, University of Kentucky, Lexington, KY 40506, USA*
[c] *Department of Chemistry, Columbia University, New York, NY 10027, USA*

† Electronic supplementary information (ESI) available. CCDC 1554121 and 1554122. For ESI and crystallographic data in CIF or other electronic format see DOI: 10.1039/c7cp03774k

‡ Current address: KAUST Solar Centre, King Abdullah University of Science and Technology, Thuwal, Saudi Arabia.

electronic coupling. The electronic coupling requirement is fairly complex and is best evaluated on a case-by-case basis; however, generally it is required for delocalization of the singlet exciton, and the output description of the singlet wavefunctions (composed of exciton resonance, charge resonance, and doubly-excited configurations) defines the rate of conversion into the correlated triplet pair state, ^{1}(TT), which is the pre-eminent intermediate leading to separated triplets.[4,5,9–11] These aspects of the electronic structure are highly dependent on molecular geometry, inciting design criteria for intermolecular packing in the solid state or conformational landscapes of dimers in solution. It has recently been shown that triplet separation occurs through multiple spin-correlated energy transfer steps of overall singlet character prior to spin decoherence which leads to isolated triplets.[11,12]

Thus far, the library of materials that undergo singlet fission has remained relatively limited despite recent insights into the singlet fission mechanism. Some families of compounds include: 1,3-diphenylisobenzofuran,[13,14] carotenoids,[15] rylenes,[16,17] thiophene dioxide-based polymers,[18] and 3,6-bis(thiophen-2-yl)diketopyrrolopyrrole films.[19] However, the vast majority of materials studied to date have been based on the acene family of chromophores, namely tetracene, pentacene, and hexacene, due to the facile nature of singlet fission in an assortment of material forms. Among these chromophores, pentacene derivatives have shown the fastest rates for singlet fission, and triplet yields consistently near 200%—primarily due to the favorable alignment of the singlet excited state and $2 \times T_1$. These observations have been made in a variety of contexts such as concentrated solutions,[20] films,[6,20,21] oligomers,[22] suspended nanoparticles,[10,12,23] and dimers in solution.[24–26] Despite the high singlet fission yields characteristic of the acene family, their poor photostability and limited spectral tunability remain a restriction for eventual device implementation. Improvements to the solubility and photostability of pentacene and tetracene, necessary for their large scale application, have somewhat been realized by functionalization with side-groups such as bis(triisopropylsilylethynyl) (TIPS) and bis(triisobutylsilylethynyl) (TIBS).[27] However, there is a growing need to improve upon these challenges by extending the library of singlet fission-enabled compounds beyond the acene family.

Covalently-linked dimers have been a novel platform for investigating the singlet fission mechanism and its molecular dependencies. They are the minimal unit required for singlet fission, and the photophysics of single pairs of chromophores tends to be much simpler to disentangle without complications related to morphology, exciton diffusion, and exciton–exciton annihilation common in crystalline and amorphous materials. Furthermore, their transient spectra and photoluminescence can be directly compared against suitable monomer spectra for reference, allowing for both the initially excited singlet exciton and the correlated triplet pair state to be evaluated directly. For example, recent studies of tetracene–pentacene heteroacene dimers illuminate the relative monomer character within the singlet excitation unambiguously through ground state bleach signatures in transient absorption.[28,29] Since pairwise interactions drive singlet fission, chemical design incorporated into dimers also yields valuable insights into the appropriate conformational characteristics which give rise to facile singlet fission and/or traps which may hinder triplet formation. One relevant example is excimer-like intermediates which have separately been reported as traps which compete against internal conversion to the ^{1}(TT) state,[14,30,31] and as an intermediate leading to ^{1}(TT).[16,19] These excimer-like species can be viewed as a displaced minimum on the excited state potential energy surface of ''pre-associated'' dimers,[32–34] and are analogously described in molecular crystals as excimer excitons which are characterized as a displaced minimum due to a balance of the attractive excimer interaction potential and repulsive intermolecular potential.[35] The role of these excimer exciton intermediates in singlet fission is still a matter of debate, but seems to be dependent on the particular system. For those systems that still exhibit singlet fission through an excimer-like intermediate, the energetics relative to the higher-lying Franck–Condon region may incidentally be favorable, or the excimer conformation may couple more strongly to the correlated triplet pair state. Detailed calculations of the energies and coupling strength between the excimer exciton state and ^{1}(TT) are necessary to predict the rate for singlet fission in such a scenario.[30]

While polyacenes seem to be the choice class of molecules for efficient fission, there is a need to expand the current library of compounds in order to increase the diversity of options available for singlet fission-sensitized solar cells. Namely, other compounds that can complement the pentacene absorption in other parts of the solar spectrum would improve total solar light capture, and it is desirable that the molecule is robust against long-term exposure to light and oxygen compared to pentacenes. Anthradithiophenes have been shown to complement pentacene as an organic photovoltaic material, displaying high photoconductivity, notably high fluorescence quantum yields in films, and enhanced tunability of electronic properties by substitution of end-groups.[36–38] In addition, greatly improved photostability relative to pentacene derivatives has been documented.[36,38] The larger HOMO–LUMO gap of anthradithiophenes also naturally shifts the first electronic absorption typically >100 nm to the blue of its analogous pentacene derivative, presenting an opportunity to enhance overall spectral capture in the form of a binary blended sensitizer. Given these advantageous properties, some work has addressed the anthradithiophene family and other heteroatom-substituted acenes as potential singlet fission candidates. Interestingly, it was found that the exothermicity between S_1 and $2 \times T_1$ was significantly larger than typical acenes (0.58 eV),[38,39] suggestive of potentially high singlet fission efficiencies.

In this work we evaluate the optical properties and photophysics of a difluorinated anthradithiophene, functionalized with solubilizing triisobutylsilylethynyl (TIBS) groups (ADT-TIBS-F: ''ADT''), along with a (dimethylsilyl)ethane-linked dimer composed of two ADT monomers ((ADT-TIBS-F)$_2$-DMSE: ''2ADT'') in order to further investigate the impact of functionalization on singlet fission properties. All anthradithiophene chromophores investigated here are in their isomerically-pure *syn* form (sulfur atoms *syn* to one another), and Fig. 1a shows the chemical structures for both ADT and 2ADT. The effect of solvent polarity

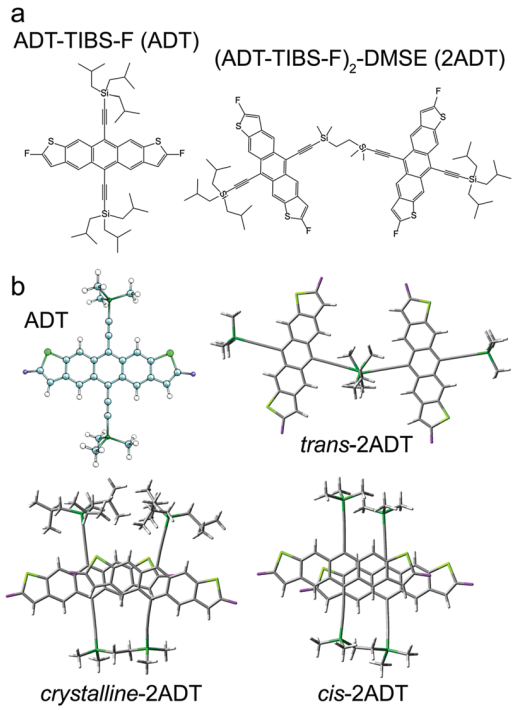

Fig. 1 (a) Chemical structures and (b) calculated geometries for ADT-TIBS-F (ADT) and (ADT-TIBS-F)$_2$-DMSE (2ADT). The 2ADT crystal structure is also shown in (b) for comparison. ADT is shown as a ball-and-stick structure in (b) for a detailed atomistic view while 2ADT is given in tube form for simplicity.

on the photophysics of 2ADT is addressed by first identifying the key intermediates formed following photoexcitation, and determining their rates of formation by a combination of steady-state absorption and fluorescence spectroscopy, time-resolved fluorescence (TRF), and femtosecond transient absorption (TA) spectroscopy. Finally, the role of excimer-like intermediates in singlet fission is discussed in the context of 2ADT.

Methods

Experimental methods

ADT and 2ADT were synthesized by re-silylation of the as-prepared pure *syn* isomer, using the methods described in ref. 40 and briefly given in the ESI.†[40] For steady-state absorption and fluorescence measurements, the optical density (OD) of all samples was kept below 0.1 in a cuvette with 1 cm pathlength (<4 μM concentrations). Steady-state absorption measurements were carried out on a Cary 6000i UV-vis-NIR spectrometer, and fluorescence spectra were collected on a Horiba PTI QuantaMaster 400 fluorometer using 0.38 mm slit widths for both excitation and emission. Fluorescence quantum yields were determined by comparison against the reference dye rhodamine 6G, and all reported fluorescence spectra are intensity corrected. Time-resolved photoluminescence was performed *via* time-correlated single photon counting on a Horiba Deltaflex spectrometer equipped with a 507 nm DeltaDiode pulsed diode laser for excitation. The instrument response was recorded by collecting scattered light from solvent, and it was used in reconvolution analysis to appropriately extract and fit the fluorescence decay. Single fluorescence decay acquisitions were collected up to 20 000 counts at the maximum and each reported profile is an average of 4–5 trials; time-resolved fluorescence maps were collected with a 5 nm step size and a 1 hour collection time for each wavelength. For absorption and fluorescence spectra taken at 77 K, samples were loaded into a Janis ST-100 liquid nitrogen cryostat.

Narrowband transient absorption spectroscopy was performed on a Helios transient absorption spectrometer (Ultrafast Systems) with a Coherent Libra Ti:sapphire regenerative amplifier system operating at 1 kHz repetition rate at 800 nm. The output was used to pump both a Coherent OPerA Solo optical parametric amplifier (OPA) for generation of the pump beam, and a white light generation stage in the Helios to generate the probe beam in either the visible or near-IR (NIR) regions. All TA measurements were carried out with the pump–probe polarization angle set to magic angle (54.7°), and the pump pulse energy was kept to 30–35 nJ per pulse. The sample was placed in a 1 mm pathlength cuvette with an OD of ~0.3. The TA spectra were collected with exponentially increasing time steps starting at a step size of 30 fs, and the time range extended to >7 ns. The time resolution of the system is approximately 70 fs. Each point in the TA scans recorded was an average of 500 ΔA spectra, and the reported TA data sets taken in the visible region are an average of approximately 20 scans while data taken in the NIR are an average of approximately 50 scans. TA spectra are presented as $\Delta A = A_{\text{unpumped}} - A_{\text{pumped}}$ yielding ground state bleach (GSB) and stimulated emission (SE) signals negative, and excited state absorption (ESA) and photo-induced absorption (PIA) signals positive. Global analysis of the chirp-corrected TA data was performed using the Glotaran program.[41] Triplet sensitization measurements were performed with a sample OD of ~0.3 in a 2 mm cuvette. Anthracene was dissolved in the toluene solution to a concentration of 20 mM, and solutions were degassed with argon prior to the measurements. An excitation wavelength of 360 nm was used to excite anthracene, and the time delay was controlled electronically resulting in a final time resolution of ~1 ns.

Computational methods

Calculations were performed on ADT and 2ADT structures with abbreviated TIBS groups incorporating methyl substituents in place of isobutyl groups for computational feasibility (Fig. 1b). We note that the substitution leaves the electronic properties of the ADT core intact as the TIBS substituents are not a part of the electronic system. The geometry of the *cis* 2ADT conformer is affected by the substitution particularly in the relative long axis angle between ADT monomers and therefore the alignment of π orbitals as evidenced by comparison with the crystal structure shown in Fig. 1b. However the intermolecular distance between ADT chromophores is only marginally affected, allowing for at least a qualitative evaluation of the π-stacked *cis* conformer. All calculations were carried out using the Gaussian 09 suite.[42] Ground state geometry optimizations and harmonic frequency calculations were performed using density functional theory (DFT) with the CAM-B3LYP functional[43] utilizing the 6-31+G(d)

basis set for ADT calculations, while 6-31G was used for 2ADT due to its large size. Excited state optimizations, vibrational frequencies, and vertical excitation energies were calculated with time-dependent density functional theory (TDDFT) again with the CAM-B3LYP functional and identical basis sets as for ground state calculations.

Results and analysis

Computational results and crystal structure

The optimized ground state structures for ADT and 2ADT are shown in Fig. 1b. The ADT monomer structure is fairly rigid, and its only conformational freedom is in the alignment of the remote alkyl side groups which minimally affect the optical properties of the ADT core. Nevertheless, both trimethylsilyl groups stagger the ADT plane to minimize the proximate sterics with the ADT π-system, leading to an eclipsed conformation of the two trimethylsilyl groups. The (dimethylsilyl)ethane (DMSE) linker in 2ADT is flexible enough to allow the ADT π-systems to interact thereby stabilizing the *cis* face-to-face conformation, however, with a steric penalty associated with the terminal TIBS groups and a deformation of the Si–C≡C bond angle of one ADT unit to 172°. The ADT cores are slipped along the long axis by approximately the length of the DMSE linker, or ∼3.8 Å, and the distance between cores is calculated to be approximately 3.5 Å. The 2ADT *cis* conformer is indeed adopted in the crystalline phase as demonstrated in Fig. 1b. Comparing the full dimer structure revealed in crystalline 2ADT with the calculated *cis* conformer of 2ADT, the π-stacking is altered due to a shift in the relative angle between ADT long axes from approximately 3° (*cis*-2ADT) to 23° (crystalline-2ADT). The shift in alignment is primarily due to the bulky TIBS groups (which are not represented in the *cis* calculated structure) which force a larger slip between ADT chromophores to accommodate the high degree of sterics. However, since the ADT cores are bound by the ethylsilyl bridge opposite the TIBS substituents, and the bridge length is shorter than the induced slip by ∼1 Å, the ADT cores are forced out of alignment. The sterics are relieved in the *trans* conformation (Fig. 1b, bottom) where the ADT cores are separated by >10 Å and staggered out of plane along the perpendicularly oriented DMSE linker by 3.9 Å. The π–π interaction of the *cis* conformer stabilizes its energy making it the global energy minimum by 13.1 kJ mol^{-1}. However, given the larger entropy associated with the extended *trans* conformer, the total free energy is lower by 6.34 kJ mol^{-1} at room temperature, making it the global free energy minimum. We note that these values are for calculations of the gas-phase molecule, without taking into account solvation effects. Nevertheless, based on these results we can qualitatively expect the likely presence of either or both of these conformers in solution. The *cis* conformation adopted in the crystalline phase however suggests that the *cis* conformer is dominant in solution prior to aggregation and crystallization.

Previously, the phosphorescence spectrum of an analogous ADT compound, *anti* ADT-TIPS, was reported and shown to exhibit a maximum at ∼1525 nm, placing the triplet state 6560 cm^{-1} above the ground state.[38] The triplet energy calculated at the ground state geometry (vertical excitation energy) for *syn*-ADT here was found to be 6553 cm^{-1} at the DFT//CAM-B3LYP/6-31+G(d) level of theory—in good agreement with the experimental value for *anti* ADT-TIPS. When the vertical excitation energies are scaled to match the S_0–S_1 excitation energy of ADT in solution (scale factor = 0.981), this value is reduced to 5840 cm^{-1}. Therefore the computed singlet fission driving force for ADT, $\Delta E_{SF} = 2E_{T1} - E_{S1}$, is ∼ −7000 cm^{-1}. The magnitude of this value is even larger than the reported ΔE_{SF} ∼ −4700 cm^{-1} for *anti*-ADT, and significantly more exothermic than those reported for acenes to date; an effect expected to reduce the singlet fission rate due to population and subsequent relaxation from the dense subset of degenerate vibrational states within the ^{1}(TT) manifold at the S_1–^{1}(TT) state crossing.[9,44] Despite an expected reduction in rate, the large exothermicity should still allow singlet fission to dominate the photophysics of the dimer barring geometric/coupling dependencies. A notable example of how the singlet fission rate scales as a function of exothermicity is through comparison of crystalline pentacene and hexacene. In that case, pentacene undergoes singlet fission in ∼80 fs with ∼1000 cm^{-1} exothermicity whereas in hexacene it occurs in 530 fs with a significantly larger exothermicity of >4000 cm^{-1}.[21,44,45] Furthermore, recent theoretical work shows that when the phonon bath is appropriately accounted for, the singlet fission rate remains ∼1 ps^{-1} down to at least ΔE_{SF} = −6500 cm^{-1}.

Steady-state spectroscopy

The absorption and fluorescence spectra for ADT (dashed) and 2ADT (solid) are shown in Fig. 2a in both toluene and acetone. In toluene, the visible absorption peaks at 18 940 cm^{-1} (528 nm) with a fluorescence maximum at 18 730 cm^{-1} (534 nm) yielding a Stokes shift of ∼210 cm^{-1}. Characteristic vibronic activity is found similar to tetracene and pentacene, with extended progressions in skeletal ring modes centered at +1400 cm^{-1}. The absorption and fluorescence spectra of the 2ADT dimer are both shifted to the red by ∼50 cm^{-1}, and the absorption spectrum has a weak tail extending to the red of the primary electronic origin feature.

The spectra in acetone are qualitatively similar to the nonpolar toluene spectra, however there are several notable differences. Firstly, the spectra for both ADT and 2ADT are blue-shifted by over 100 cm^{-1}, and the absorption peaks of 2ADT are significantly broadened compared to the monomer. Further, the tail extending to the red of the primary origin peak is much more pronounced in 2ADT compared even to the toluene spectrum. Another notable characteristic of the dimer spectrum is the relative intensity of the origin band to the first vibronic sub-band, I_{0-0}/I_{0-1}. In the case of toluene the ratio is 1.54 while in acetone it is decreased to 1.20. The appreciable intensity difference in the dimer is suggestive of a face-to-face conformation and is characteristic of excitonic interactions in H-type aggregates.[46,47] The smaller the I_{0-0}/I_{0-1} ratio compared to monomer spectra, the stronger the excitonic interaction between chromophores in

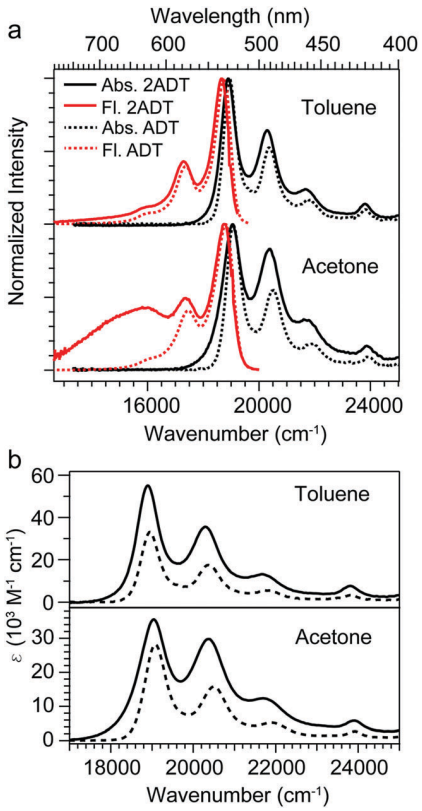

Fig. 2 (a) Absorption (black) and corrected fluorescence (red) spectra for ADT (dashed) and 2ADT (solid) in toluene and acetone. Fluorescence spectra were recorded following excitation at the absorption maxima. (b) Molar extinction spectra for ADT (dashed) and 2ADT (solid) in toluene and acetone.

the dimer, and the effect is clearly seen in going from ADT to 2ADT in both solvents. With these effects in mind, a comparison between 2ADT spectra suggests fairly significant excitonic coupling in acetone solvent. Lastly, comparing the fluorescence spectra of ADT to 2ADT reveals a broadened, red-shifted band peaking near 15 800 cm^{-1} and extending well past 13 000 cm^{-1}. The existence of such broad emission only in a polar solvent suggests charge-transfer (CT) character of the emitting state. This dual emission in acetone can then be tentatively assigned to either: (i) a single conformer with an excited state incorporating CT character, or (ii) a mixture of *trans* and *cis* conformers which both exhibit characteristic spectra, with one of which being stabilized by polar solvent. We will return to this point in the Discussion section.

The molar extinction spectra for ADT and 2ADT are shown in Fig. 2b. In toluene, the ADT dimer shows about twice the total extinction of the monomer as expected for a weakly or non-interacting dimer system. In acetone however, the peak extinction of 2ADT at the absorption origin is significantly smaller than twice that of ADT, likely due to the extensive spectral broadening apparent which itself signals non-trivial excitonic interactions between chromophores. The excitonic coupling splits the "monomer" bands leading to an overall decrease in peak intensity, but still conserves the integrated extinction over the entirety of the electronic absorption. Table 1

Table 1 Spectroscopic properties of ADT and 2ADT in toluene and acetone

Toluene	ε^a (M^{-1} cm^{-1})	Φ_F	τ_1 (ns)	τ_2 (ns)
ADT	33 175	0.76	—	8.98 ± 0.02
2ADT	55 180	0.11	1.75 ± 0.01 (0.93)	8.20 ± 0.51 (0.07)
Acetone	ε^a (M^{-1} cm^{-1})	Φ_F	τ_1 (ns)	τ_2 (ns)
ADT	28 200	0.69	—	9.22 ± 0.04
2ADT	35 585	0.03	0.64 ± 0.00 (0.68)	9.59 ± 0.13 (0.32)

[a] Taken at the wavenumber of the absorption maximum.

gives the molar extinction coefficients at the absorption maxima for all four scenarios, along with fluorescence quantum yields, Φ_F. The fluorescence quantum yield of ADT is in agreement with the analogous *anti*-ADT-TIPS-F reported previously,[37] here reaching 0.76 and 0.69 in toluene and acetone respectively. Going to the dimer however, the total Φ_F is reduced to 0.11 and 0.03 respectively. The reduction implies the introduction of new non-radiative pathways when covalently linking the two ADT chromophores, likely either singlet fission or some other form of internal conversion. This will be explored further in the following sections. Absorption and fluorescence spectra, along with photophysical characterization of 2ADT in cyclohexane, THF, and dichloromethane are given in the ESI.†

Absorption spectra extended through the UV region are shown in Fig. 3 for ADT (dashed) and 2ADT (solid) dissolved in 2-methyl THF (2-mTHF) at room temperature (top) and 77 K (bottom). The room temperature spectra are nearly identical to the toluene spectra given in Fig. 2, and again display qualitatively similar spectra between the monomer and dimer. Extending past the $S_0 \rightarrow S_1$ region reveals multiple absorptions throughout the UV-visible region. To aid in assigning the individual electronic absorptions, TDDFT vertical excitation calculations were performed on ADT, and the predictions are shown as sticks under the cold 2ADT spectrum at the bottom of Fig. 3 and in the inset (calculated spectrum scaled to match the S_0–S_1 transition).

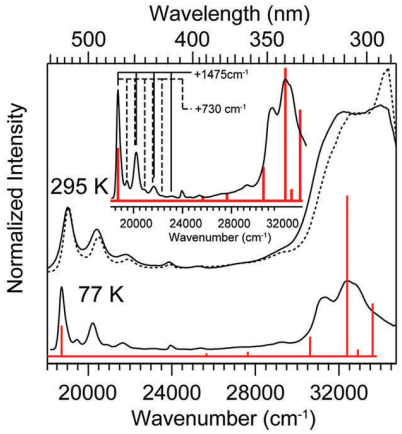

Fig. 3 Extended absorption spectra for ADT (dashed) and 2ADT (solid) in 2-methyl THF at 295 K (top) and 77 K (bottom), with TDDFT//CAM-B3LYP scaled electronic absorption predictions shown as red sticks. The inset shows the fit to experiment and assignable vibronic progressions at 77 K.

While the TDDFT results are found to generally overestimate the excitation energies, the relative intensities and ordering help in assigning particular electronic transitions to distinct features in the experimental spectrum. For example, the small band at 23 920 cm^{-1} is assigned to the long-axis polarized $S_0 \rightarrow S_2$ absorption, and the peak near 27 000 cm^{-1} can be assigned to the $S_0 \rightarrow S_3$ transition. Likely the band at $\sim$29 250 cm^{-1} is the S_0–S_4 origin, however given the density of electronic transitions in the far UV region, assignments can only be made on a tentative basis at this point. The primary molecular orbitals and transition dipole moments associated with the first four electronic transitions are given in the ESI† (Fig. S3). Several large absorptions are predicted in the $\sim$300 nm region, yielding reasonably good agreement with the experimental spectrum and enabling an estimate of the number of excited states accessible in that region. This information assists in assigning particular excited-state absorption features in transient absorption data as demonstrated below. The vibronic activity is substantially more resolved at low temperature (Fig. 3, bottom), and the tie lines in the inset show two sets of vibrational progressions. At least three members of the high frequency $\sim$1475 cm^{-1} band are found, and up to five bands of the 730 cm^{-1} progression can be tracked signaling a fairly large geometry change in that coordinate(s) upon excitation to S_1. A detailed Franck–Condon simulation with relevant vibrational assignments is given in the ESI† (Fig. S4), and is found to match the experimental absorption spectrum remarkably well.

Time-resolved fluorescence

To further address the dramatic reduction of Φ_F in 2ADT, time-resolved fluorescence (TRF) was performed in both solvents and the results are given in Fig. 4 and Table 1. The fluorescence decays were collected at the fluorescence maximum of each individual sample (Fig. 2), and the error is reported as the standard deviation of four individual measurements. The fluorescence decay of ADT could be fit with a single exponential with a time constant of $\sim$9 ns. The reduced quantum yield in 2ADT is clearly borne out in the TRF profiles which reveal biexponential kinetics, with the faster component decaying with a time constant τ = 1.75 and 0.640 ns for toluene and acetone respectively. The longer-lived component decays with a similar time constant as the ADT monomer, and represents a much smaller fraction of the population (Table 1). Given the dilute μM concentrations used for these measurements and general lack of concentration dependence, we can definitively rule out bimolecular excimer formation or aggregation-induced internal conversion as quenching mechanisms contributing to the biexponential dynamics. Alternatively, the profiles could resemble delayed fluorescence which can be expected following singlet fission and subsequent triplet fusion to re-form the initial singlet state. However, in this case such a scenario is unlikely due to the exceedingly large energy difference between $2T_1$ and S_1.

Transient absorption spectroscopy

The TRF results clearly demonstrate the onset of a non-radiative pathway present in the covalently-tethered ADT dimer,

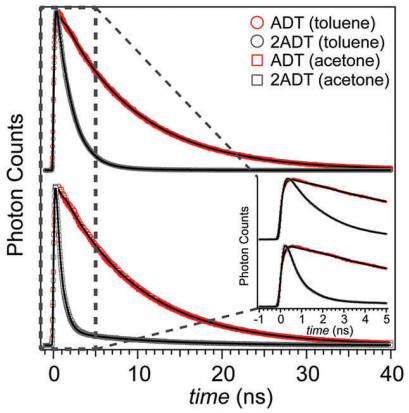

Fig. 4 Time-resolved fluorescence decay profiles measured at the fluorescence maxima of ADT (red) and 2ADT (gray) in toluene (top) and acetone (bottom) following excitation at 507 nm. The fits are shown as black lines.

and a difference of nearly a factor of 3 in their rate constants highlights its strong solvent dependence. To identify the mechanism and all formed intermediates, we performed transient absorption on ADT and 2ADT in both toluene and acetone. The TA spectra of ADT serve as a reference for making spectral assignments in 2ADT spectra, and considering that singlet fission requires two or more monomers, only singlet features are expected in those sufficiently dilute ADT solutions. For all TA data reported here, the pump wavelength was set to the absorption maximum of each sample.

The time-resolved TA spectra for ADT in toluene are shown in Fig. 5a and b. At early times, the largest feature appears between the absorption and fluorescence maxima at 18 870 cm^{-1} and is assigned to overlapping $S_0 \rightarrow S_1$ ground state bleach (GSB) and $S_1 \rightarrow S_0$ stimulated emission (SE) features. The SE vibrational sub-band is clearly observed near 17 350 cm^{-1} and undergoes a dynamic Stokes shift within a few picoseconds. Several excited state absorption (ESA) signatures originating from S_1 are detected at 7970 cm^{-1} ($S_1 \rightarrow S_3$), 11 900 ($S_1 \rightarrow S_4$), 13 600 ($S_1 \rightarrow S_5$), 19 800, and 22 000 cm^{-1}. Their assignments were made by inspection of the absorption spectra in toluene and 2-mTHF (Fig. 3). As expected, all S_1 features decay similarly over the course of the measurement and no new features, or intermediates, are observed. The SE and ESA bands all decay at roughly the same rate as the GSB confirming that radiative decay to the ground state is the dominant excited state relaxation channel.

In the first few picoseconds, quantum beats are observed near the center of the GSB/SE feature at 18 870 cm^{-1} as shown in the inset in Fig. 5b. The coherence dephases within $\sim$4 ps, and following extraction of the signal *via* a biexponential fit over this time range, a Fourier transformation reveals its frequency as 240 cm^{-1}. This frequency matches closely the ADT core breathing mode predicted by the Franck–Condon prediction shown in Fig. S4 (ESI†), and given the large Franck–Condon factor for this excitation we can safely assign the vibrational coherence to this mode. A subtraction of the early time population dynamics over the entire probe range reveals that the coherence is highly localized to the GSB region, and its

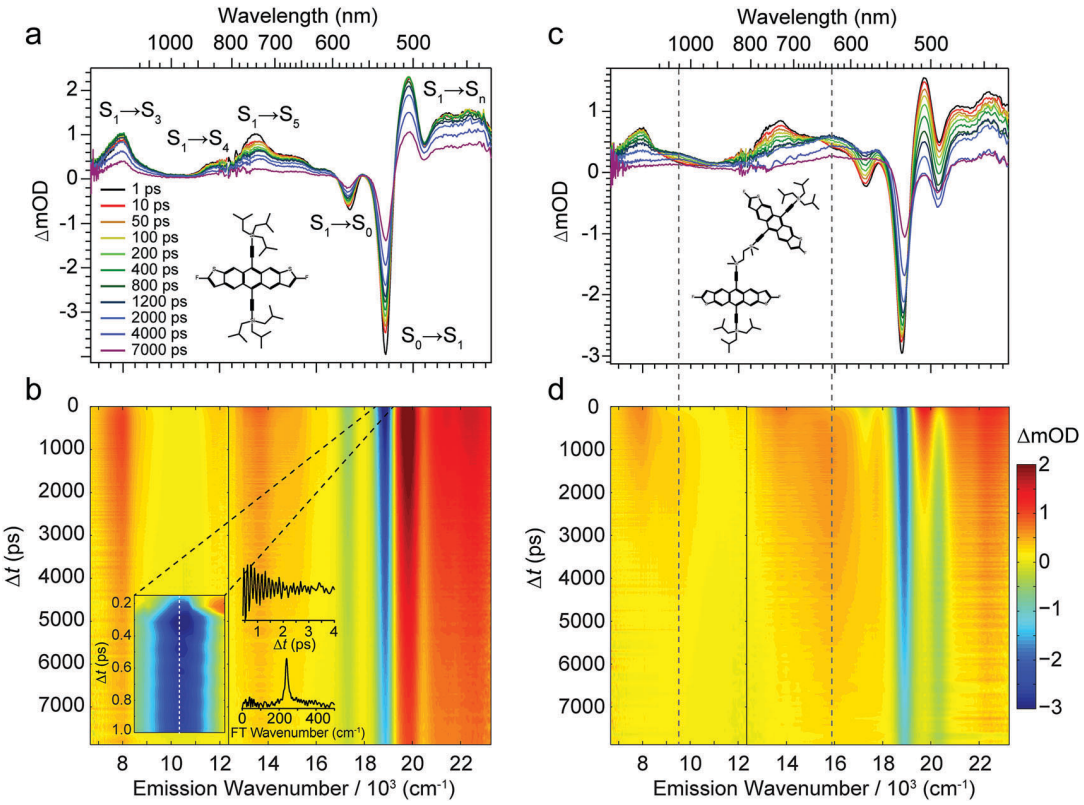

Fig. 5 Transient absorption spectra of ADT (a and b) and 2ADT (c and d) in toluene. Dashed lines in c and d indicate the positions of features formed. The inset in (b) shows vibrational coherence at early time along with its Fourier transform. The pump excitation wavelength was set to the visible absorption maximum in both solvents.

amplitude has a node at the peak of the ADT absorption unambiguously exposing the location of the coherence on the ground electronic state (ESI†). Despite being completely buried under the lineshape in the absorption and fluorescence spectra, this mode can be observed and unambiguously assigned—illustrating the power of coherence analysis in tandem with *ab initio* Franck–Condon simulations.[48]

The 2ADT spectrum (Fig. 5c and d) shows analogous spectral features at early times, but all of the S_1 bands decay away into two new features centered at 9600 and 16 000 cm^{-1}. These are indicated by dashed lines in Fig. 5c and d. It is evident from the surface in Fig. 5d that the decay of S_1 SE and ESA correlate well with the growth of the intermediate photo-induced absorption (PIA). All that remains after $\sim$3 ns are these PIAs and residual ground state bleach. Interestingly, the decay of the intermediate and GSB appears to occur faster than the monomer radiative decay.

The TA results for ADT and 2ADT in acetone solvent are given in Fig. 6a, b and c, d respectively. Very little difference is found for ADT and all representative spectral bands can be assigned as before. Some differences emerge in the GSB recovery time though, where in acetone $\sim$56% of the population has been recovered at 7 ns *versus* 65% in toluene. The 2ADT spectrum is qualitatively similar to that in toluene except that the GSB features are markedly broadened. The formation of an intermediate state occurs more rapidly in this case in accordance with TRF, and the amplitudes of the intermediate features are significantly larger in acetone compared to toluene. The S_1 SE and ESA features decay within 1 ns to form the intermediate, which subsequently relaxes to the ground state as shown in the correlated GSB recovery.

At this point we can speculate as to the identity of the intermediate species formed prior to decay to the ground state. The most tantalizing possibility is that the features in the 2ADT spectra could be associated with triplets or the correlated triplet pair state populated through singlet fission, yielding signatures of $T_1 \rightarrow T_n$ photo-induced absorption. While the timescale for formation is much slower than the typically picosecond or sub-picosecond timescales for pentacene homodimers with similar intermolecular separation,[24,26] the timescale is still much faster than that anticipated for intersystem crossing, and the dynamics occur only when two ADT chromophores are brought into close proximity. The expedited decay to the ground state would then be associated with triplet–triplet annihilation, as has been extensively documented for covalently-linked acene dimers.[24–26,28] Assuming this scenario, 2ADT would not be a choice candidate for singlet fission in solution given that the triplet yield would be far from quantitative, solvent-dependent, and the triplet recombination rate is not sufficiently longer than the fission rate.

Alternatively, the intermediate could be a trap state which then decays to the ground state non-radiatively. Such a case can occur with formation of excimer-like states, where in the case of covalently-linked dimers that are pre-associated in the

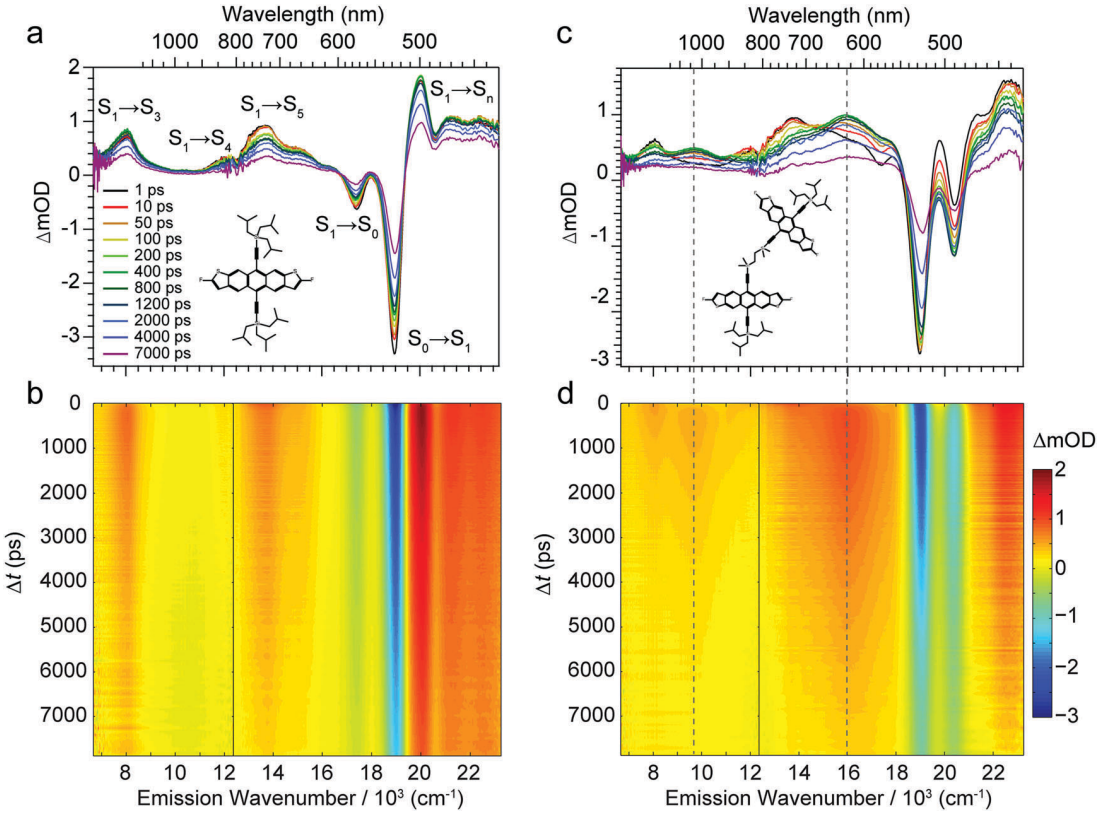

Fig. 6 Transient absorption spectra of ADT (a and b) and 2ADT (c and d) in acetone. Dashed lines in c and d indicate the positions of features formed. The pump excitation wavelength was set to the visible absorption maximum in both solvents.

ground state, such a situation can be viewed as a dramatic inter-monomer geometry change on the excited state surface (such as a large reduction in the intermolecular distance, intermolecular slip, or intermolecular torsion). In order to test these photophysical pictures, global analysis of the TA data was undertaken along with triplet sensitization measurements for recovery of the single ADT triplet spectrum.

To isolate the spectra of individual contributions to the dynamics resolved in TA, global analysis employing a sequential model was utilized. The ADT TA data was fit with three primary components, and the results are shown in Fig. 7a and b. The fastest component, defined as EAS1, decays in 3 (0.48) ps in toluene (acetone) and is assigned to vibrational/solvent relaxation contributing to the Stokes shift. The SE features peaking at 18 870 (18 990) and 17 390 (17 540) cm^{-1} clearly red-shift as EAS2 is formed. To appropriately capture the spectral evolution, EAS2 associated with a time constant of 190 (100) ps was required. Comparing EAS2 against EAS3 reveals differences predominantly in the $S_1 \rightarrow S_3$ and $S_1 \rightarrow S_5$ regions with a growth in the former and decay in the latter. As such, it can be ascribed to slow vibrational relaxation within the S_1 manifold which these ESA bands are particularly sensitive to presumably due to large displacements between S_1 and the corresponding upper excited states along the coordinate(s) of relaxation. Finally, EAS3 yields time constants nearly identical to those extracted from TRF and are therefore assigned to radiative decay to return population to the ground state. It is noted that the time constant was fixed in the case of acetone to adequately capture a small fourth component which extends well past the time range of the experiment. The fit was sufficient when EAS4 was set to 20 ns or longer, and we assign this residual population to triplets formed by intersystem crossing based on the characteristically long lifetime of the population, complete lack of SE signal, and comparison with triplet sensitization measurements (see below).

With the dynamics of ADT assigned, we are now in a position to address the photophysics and intermediate in 2ADT. If the intermediate formed is the correlated triplet pair, the spectral features should resemble $T_1 \rightarrow T_n$ PIA signatures. Therefore we must find an adequate reference which yields pure triplet TA spectra. To do this, we generated triplets in solution by dissolving an excess of anthacene and pumping it directly to eventually form triplet anthracene. Probing at long times (10–100 μs) ensures that triplet–triplet energy transfer to ADT has occurred, leaving behind ADT triplets which are then probed in the visible region. Fig. 7c shows the time-integrated triplet spectra of ADT (red) and 2ADT (black) over 10–100 μs. The bleach is found as expected indicating successful triplet generation on ADT/2ADT, and a broad PIA spanning 17 000–23 000 cm^{-1} is the only triplet band in the spectrum. The feature is disrupted by the vibrational bleach signatures of the singlet and appears to be relatively broad and structureless otherwise. Furthermore, it is in the vicinity of the $S_1 \rightarrow S_n$ ESA

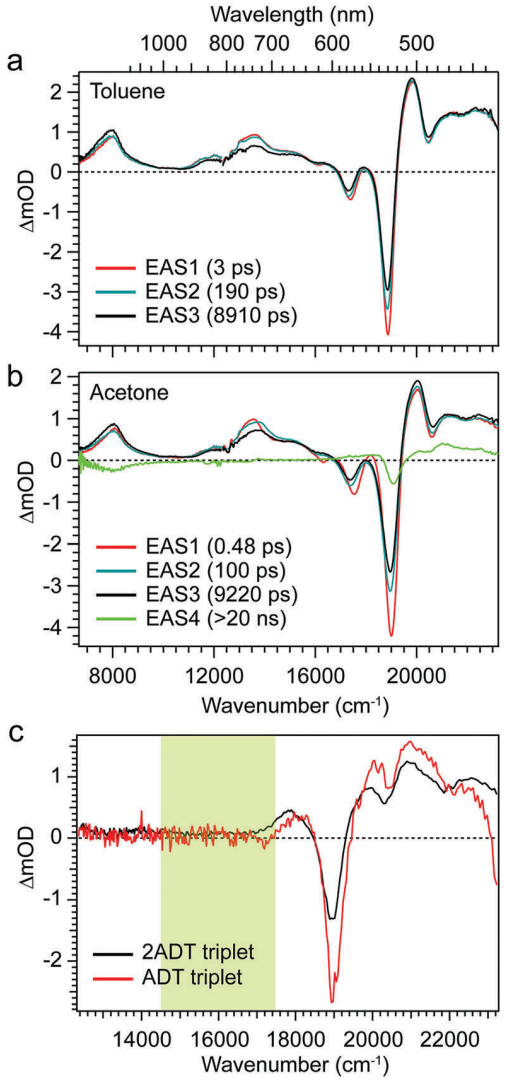

Fig. 7 Global analysis results for ADT in (a) toluene and (b) acetone. The evolutionary-associated spectra (EAS) were generated by global fit of the data to a sequential model. (c) Triplet spectra of ADT (red) and 2ADT (black) from triplet sensitization in toluene.

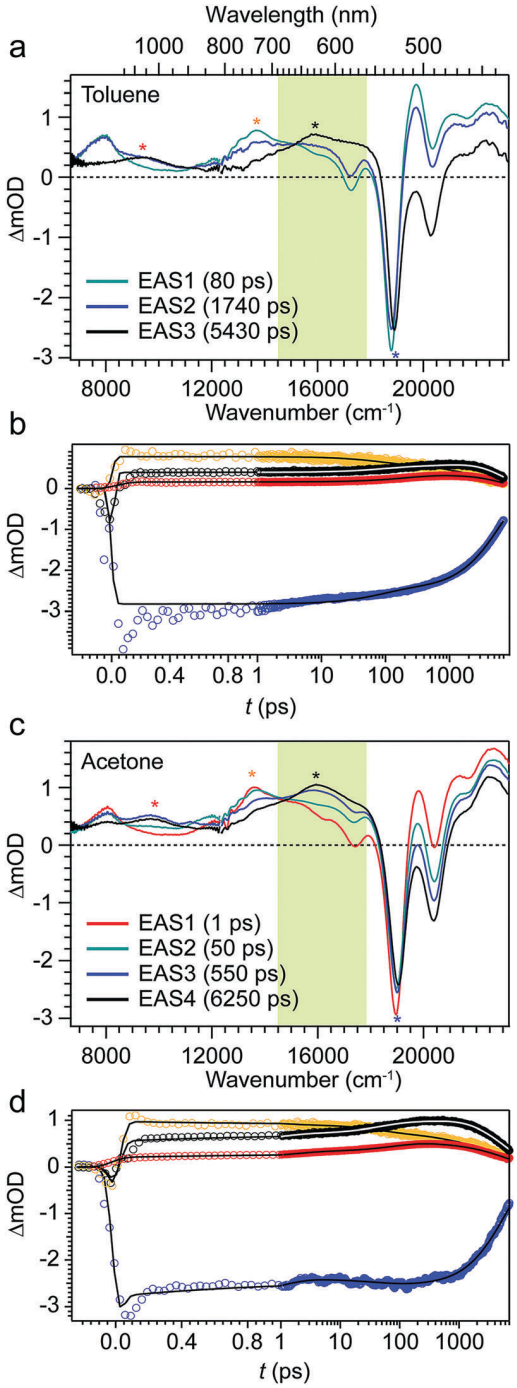

Fig. 8 Global analysis results for 2ADT. Evolutionary-associated spectra in (a) toluene and (c) acetone along with (b and d) kinetic traces (circles) and fits from global analysis of the data using a sequential model. The spectral positions of the represented kinetic traces are given as colored asterisks in (a and c).

region in both ADT and 2ADT complicating a clean identification of triplets or the correlated triplet pair in the ultrafast TA measurements. However, the sensitization measurements report the absence of any signal in the region of the intermediate absorption (highlighted green) unambiguously indicating that the intermediate population formed in TA is not due to triplet/correlated triplet pair formation, precluding singlet fission as the primary non-radiative decay channel.

With the compelling results of these control experiments in mind, we turn back to the dynamics of 2ADT. The global analysis results employing a sequential model are shown in Fig. 8a and b for 2ADT in toluene and c and d in acetone. The TA data were fit with three components for toluene data and four for acetone, with the difference being associated with the fast vibrational relaxation assigned as before and is inconsequential to the dynamics of interest. EAS1 (EAS2) in toluene (acetone) retains the expected ADT singlet features similar to Fig. 7, including the vibrational side-bands in SE and the multitude of singlet ESAs. We attribute this again to slow vibrational relaxation within S_1. The next component (blue) decays with the characteristic timescale for formation of the intermediate. The last component represents the spectrum of the formed species along with the remaining bleach

and some residual PIA amplitude past 20 000 cm^{-1}. Indeed this spectrum captures the characteristic features of the intermediate near 9600 and 16 000 cm^{-1}; the latter of which extends to the blue into the GSB region precluding determination of the full breadth of the band. By inspection though, the vibronic activity appears similar to the neighboring $S_1 \rightarrow S_5$ band prior to intermediate formation, suggesting again that the upper ESA states are identical between the two cases, but the Franck–Condon region of the upper states is displaced further from the intermediate geometry than for the locally-excited S_1 region. This observation is suggestive of a conformational change on the S_1 surface into a local minimum which is distinctly displaced from the S_1 geometry near the original S_0–S_1 Franck–Condon region—a typical signature of pre-associated "excimer" relaxation on S_1.

While it is tempting to assume that the existence of the intermediate PIA in the vicinity of the triplet region (Fig. 7c) could potentially signal a non-zero singlet fission yield, the lack of any distinctive kinetics and poor match to the 2ADT triplet spectrum thwarts this interpretation. Comparing EAS3 with the monomer EAS3 and triplet spectrum indicates less positive amplitude overlap with the GSB signal in this region, implying a simple blue-shift of the $S_1 \rightarrow S_n$ band after the intermediate is formed in accordance with the other ESA bands. Interestingly, the decay of EAS3/EAS4 to the ground state occurs in ~6 ns, comparatively faster than the radiative decay of ADT. This decay was not observed in TRF at the wavelength positions monitored in Fig. 4, where the second component of the biexponential fits were characterized by a time constant of ~9 ns. This result further indicates that the long time component in TRF is not delayed fluorescence, but a second population with emission features more akin to the monomer. The kinetics for both measurements along with the fit from global analysis is shown below each spectral series, and the position of each trace is labeled with colored asterisks in Fig. 8a and c. The growth of the state in question is clearly seen in the kinetic traces (red and black), and they correlate well with the decay of the nearby $S_1 \rightarrow S_5$ ESA (orange).

Discussion

The photophysical characteristics of ADT and 2ADT have been evaluated in detail with a combination of steady-state spectroscopy, TRF, and TA spectroscopy with the aid of computational predictions. As expected, ADT serves as a valuable reference for isolating the large number of S_1 TA signatures helping to identify the new intermediate features found when the monomers are brought into close proximity *via* the covalent bridge in 2ADT. The formation of an intermediate, according to TRF and TA, appears to be solvent-dependent and on the order of 100 s of picoseconds to a few nanoseconds. Triplet sensitization measurements proved necessary to determine with confidence that the new features formed in TA were not related to singlet fission products—a result which would have otherwise been misinterpreted given the faster GSB recovery in 2ADT which is typically a signature of triplet recombination following singlet fission.

Excimer formation and conformational heterogeneity

With the insights gained from time-resolved spectroscopy, we can now return to the results of steady-state spectroscopy and the conformational predictions discussed previously. The room temperature absorption and fluorescence spectra in acetone are again shown in Fig. 9a as a reference, and we recall that the fluorescence spectrum displays markedly different emission signatures with typical Franck–Condon emission to the blue and a broad, red-shifted portion extending past 700 nm. Fig. 9b compares these data with the ADT monomer spectra in acetone (blue) along with the 2ADT fluorescence excitation spectrum (dashed) when monitoring emission at the peak of the Franck–Condon origin transition (labeled with dashed arrow). Interestingly, the 2ADT excitation spectrum is drastically different from its absorption spectrum, instead yielding a result that closely matches the absorption of ADT monomer. Further, the fluorescence spectrum was recorded following excitation at the peak of the excitation spectrum and strongly resembles the monomer in the 17 000–20 000 cm^{-1} region.

With the "locally-excited" character of the excitation spectrum in Fig. 9b in mind, it is clear that the broadening in absorption is derived from another more dominant species in solution. To isolate that contribution, emission was recorded following excitation of the red-tail of the first absorption band (red arrow), and the result is shown in Fig. 9c (red). By exciting only at that broadened segment of the absorption band, the broadened red-shifted portion of the dual fluorescence is clearly isolated and indeed stretches some 5000 cm^{-1} in width. The strongly red-shifted and broadened emission is indicative of a strong

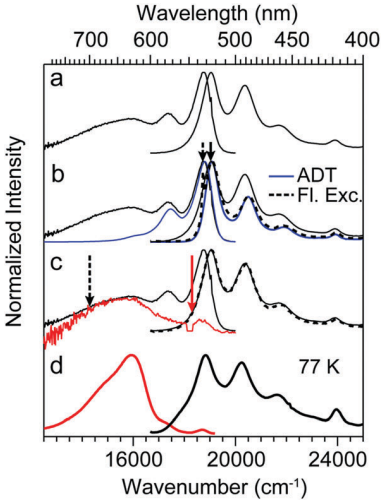

Fig. 9 Decomposition of 2ADT absorption and fluorescence spectra in acetone. (a) Absorption and corrected fluorescence spectra of 2ADT used as reference; the fluorescence spectrum was collected following excitation of the absorption maximum. (b and c) Fluorescence excitation spectra of 2ADT (dashed) monitoring the emission peak labeled with dashed arrow, and fluorescence spectrum (b, black; c, red) from excitation at the position labeled by a solid arrow. (d) Fluorescence excitation (black) and emission (red) spectra for 2ADT in acetone at 77 K while monitoring the maxima in the corresponding spectra; no spectral deviations were found with varying excitation/emission wavelengths.

excimer interaction in the homodimer, where emission occurs from a point on the excited surface well away from the Franck–Condon region. Recording the fluorescence excitation spectrum while monitoring emission near 700 nm (well separated from monomer-like fluorescence) recovered the absorption spectrum, indicating that there are two separate populations present in solution: one that yields ''monomer-like'' spectra, and one with excimer-like signatures. This is validated by isolation of the two separate fluorescence excitation spectra, indicative of distinct ground states.

The dissimilar spectral behavior of the two populations also allows us to assign them to the *cis* and *trans* conformers predicted through quantum chemical calculations, where the conformer matching closely to the monomer spectra is logically assigned to the *trans* structure since the two ADT chromophores are effectively non-interacting. The face-to-face *cis* conformer then gives rise to the observed excimer exciton formation, and the result is in line with other works on cofacially stacked π-systems.[30,31,49–52] Taken together, the behavior is apparently pervasive for face-to-face conformers stabilized by π–π interactions.

Steady-state spectroscopy reveals the presence of both *trans* and *cis* 2ADT conformers in solution, with the latter relaxing to an excimer geometry in the excited state prior to emitting. Since the population is dominated by *cis*-2ADT and the rate constants for formation of the intermediate in TA closely match the decays measured in the Franck–Condon region in TRF, it is presumed at this point that the intermediate is then associated with the excimer structure. This is explicitly borne out in spectrally-resolved TRF measurements of 2ADT in acetone as shown in Fig. 10. Fig. 10a shows early time TRF with each individual decay normalized to the count maximum. As expected based on Fig. 4, the 530–600 nm region peaks with the instrument-response function and decays at the rate of intermediate formation observed in TA. The isolated excimer emission in Fig. 9c is dominant to the red, and should peak at a rate corresponding to the decay in the Franck–Condon region. The black line in Fig. 10a marks the peak in fluorescence counts across the spectrum, and reveals that the excimer emission region is indeed delayed by roughly the formation time—confirming its assignment to the intermediate in TA measurements. Comparing the decay at 700 nm (red) and 532 nm (blue) in Fig. 10b illustrates the difference in rate for the return to the ground state between the *cis* excimer population and *trans* conformer, with the excimer state emission decaying in 5.70 ns (in accordance with TA data) *versus* the longer 9.69 ns. If the primary deactivation of the excimer state was through radiative decay, this result would be contradictory to photophysical expectations of a sufficiently longer radiative decay due to the small oscillator strength for the ground state transition. As such, we posit that the *cis*-2ADT excimer decays primarily through internal conversion while *trans*-2ADT decays radiatively. This conclusion highlights the sensitivity of the dynamics to inter-chromophoric interactions defined by the conformational landscape, resulting in conformer-specific dynamics following photoexcitation.

The relative populations of the two conformers present at room temperature are drastically different, with *cis*-2ADT dominating the population over *trans*-2ADT. The comparable intensity of the

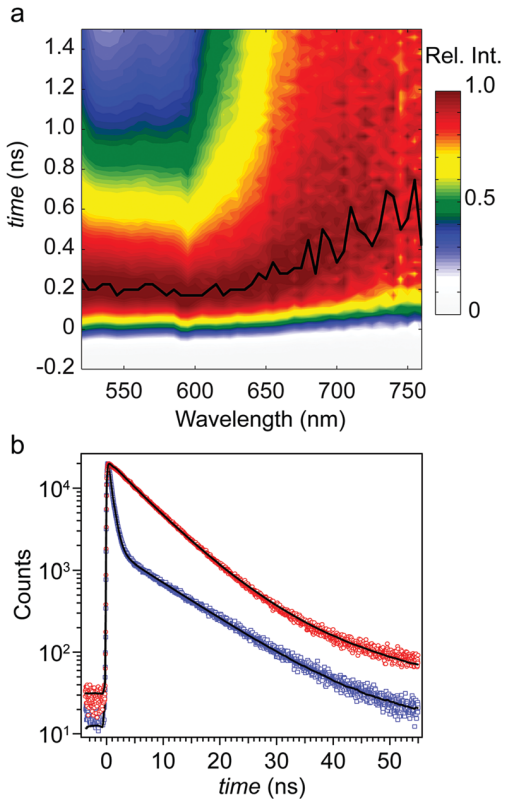

Fig. 10 (a) Time-resolved fluorescence map of 2ADT in acetone normalized to the count maximum at each wavelength. Fluorescence decays were collected every 5 nm over a 1 hour collection time. The black line indicates the time where the fluorescence was maximized. (b) Fluorescence decay profiles monitoring fluorescence at 532 nm (blue) and 700 nm (red). The biexponential fits are shown as solid lines.

trans (monomer-like) fluorescence in the fluorescence spectrum at first suggests otherwise, but we note that the fluorescence quantum yield of the non-interacting conformer is much larger than the excimer population, which also converts back to the ground state more rapidly as shown in TA and TRF. Furthermore, the marked similarity of the *cis* fluorescence excitation spectrum to the absorption spectrum in acetone indicates its dominating presence in solution, and the lack of observable stimulated emission from the *trans* conformer at long times in TA reiterates this point. We note that the presence of residual monomer in 2ADT solutions (as an impurity) can be ruled out on the basis of the difference in rates in TRF for ADT and the long component in 2ADT. Additionally, in the 7 ns TA spectrum of 2ADT (after decay of most of *cis*-2ADT population) there are no distinctive monomer signatures, particularly comparable in the $S_1 \rightarrow S_n$ high-wavenumber region.

Reflecting on the thermochemical properties of the two conformers discussed earlier, low temperature fluorescence measurements of 2ADT were undertaken in acetone to test the dependence of the two populations on temperature (Fig. 9d). Remarkably, at 77 K the entirety of the 2ADT population is funneled into the *cis* conformation yielding fluorescence and excitation spectra reminiscent of the conformer at room temperature.

No dependence on excitation wavelength was found, indicating a single population at this temperature. This observation is in agreement with computational predictions, which illustrate a significantly smaller enthalpy for the *cis* conformer over *trans* with a concomitant decrease in entropy, enabling population of the *trans* structure ($H_{cis} < H_{trans}$, $S_{cis} < S_{trans}$) at room temperature due to its overall lowered free energy. However it was shown that the *trans* conformer is still only sparsely populated at room temperature, and the reduction in temperature to 77 K scales up its relative free energy preventing its population at thermal equilibrium. We note that this correlation is made tentatively however, as alternatively the solid acetone matrix may force the ADT monomers closer to enable more facile excimer exciton formation.[35]

It is interesting to note at this point the differences in absorption and fluorescence spectra in toluene and acetone following assignment of the two clearly separate contributions in acetone. Considering the polarity difference between toluene and acetone, the large red-shifted emission in acetone would at first suggest stabilization of a charge-transfer state which then contributes more strongly to the emitting exciton state, with the dual fluorescence signaling its combined locally-excited and charge-transfer character. However, separation of the contributions in steady-state spectroscopy eliminates this possibility, and despite significant differences in intensity their spectra can also be isolated in nonpolar solvents such as toluene and 2-mTHF (ESI,† Fig. S8). The predominance of *trans* fluorescence in nonpolar solvents signals likely a larger relative population of the *trans* conformer compared to acetone (albeit still minor given a comparison of the fluorescence excitation spectra, ESI†) as toluene is more effective in solvating the aromatic surfaces of ADT through π-stacking, and the *trans* conformer exposes both sides of each ADT chromophore thereby maximizing ADT–solvent interactions. More importantly, the smaller excimer formation rate in toluene but similar internal conversion rate reduces the total lifetime of the emitting excimer state, while allowing some 1.75 ns for the initial Franck–Condon population to emit. This effect offsets the observable excimer emission at steady-state conditions. Therefore, there is a direct correlation with formation rate and observable excimer emission, in conjunction with solvent polarity proven by measurements in a variety of solvents (Fig. S1 and S2, ESI†). These results point to the role of solvent polarity in shepherding excimer formation by either stabilization of the excimer geometry or reduction of the barrier to excimer formation on the excited state surface, or by affecting the ground state pre-association directly.

Implications for singlet fission

The dynamics following photo-excitation of 2ADT have been evaluated in detail, and the two conformers identified in solution at room temperature give rise to markedly different relaxation pathways from the bright singlet state. The minor *trans*-2ADT population predominantly relaxes through radiative decay similar to its monomer precursor, while the *cis*-2ADT conformer undergoes solvent-dependent relaxation to an excimer geometry prior to internal conversion to the ground state.

The monomer-like behavior of *trans*-2ADT is unsurprising given the center-to-center distance along the short ADT axis of ~12 Å effectively eliminating through-space electronic coupling and orbital proximity required for singlet fission. The dynamics of *cis*-2ADT on the other hand are of principal interest as the chromophores are brought into close proximity yielding non-trivial π–π interactions, seemingly a candidate conformation for singlet fission. However, no singlet fission yield was detected in TA measurements. Instead only an excimer exciton population was observed. In this case it would then seem that the excimer geometry serves as a trap, preventing the population from undergoing singlet fission. While there is a precedent for this parasitic decay channel in singlet fission systems where excimer formation kinetically outcompetes singlet fission, the present scenario markedly contrasts those works in that the excimer formation in 2ADT is comparatively slower, taking place on a time scale of ~1 ns. Therefore, in this case we do not expect the excimer dynamics to be a kinetic constraint on the singlet fission yield given the rate for singlet fission in exoergic systems such as pentacene and hexacene typically occurs on a sub-picosecond time-scale. Another prospect is the thermodynamics of the excimer trap itself. If the excimer geometry was stabilized on the excited state surface to an energy below the correlated triplet pair state, $<E_{2T1}$, the population would again be trapped and singlet fission could not occur through the excimer geometry. However, in the case of ADT, the exoergicity between S_1 and $2T_1$ is larger than most singlet fission systems studied to date at an estimated range 5000–7000 cm^{-1}. We can estimate an upper limit for the stabilization, or binding energy of the excimer structure by evaluating the energy splitting of the two discernible fluorescence bands in fluorescence spectra, and by the blue-shift of the S_1 ESA bands after its formation in TA. This comparison yields $E_b^{exc} \leq 2400$ cm^{-1}, suggesting that even subsequent to excimer formation the energetics should be highly favorable for singlet fission.

Considering these aspects of the 2ADT excimer exciton state, it is clear that it should not be prohibitive in the kinetic or thermodynamic sense. The remaining factor determining singlet fission efficiency in this context is then the coupling element between S_1 and ^{1}(TT), $\langle S_0S_1|V|^1(TT)\rangle$, or between the excimer state and ^{1}(TT).[4,5] This matrix element drives singlet fission and is implicitly dependent on the π-orbital alignment of the ADT frontier orbitals, and therefore the dimer conformation. It is supposed then that in the stable cofacial conformation observed in solution, the matrix element must be negligible to preclude any singlet fission yield within nanoseconds. Extended computational investigation of 2ADT with accurate geometry optimizations and detailed electronic structure calculations at a higher level of theory would be advantageous for evaluating these couplings directly, and is beyond the scope of the present work. Nevertheless, this result highlights the chief role of the conformational landscape in activating singlet fission, even when the energetics are dramatically favorable. Given the steric influence of the bulky TIBS side groups on the ADT–ADT π-orbital alignment, 2ADT with smaller silylalkyl groups would be of interest for comparing the side group influence on *cis*-2ADT structures and their corresponding singlet fission capability.

Conclusions

The photophysics and photo-initiated dynamics of ADT and 2ADT have been investigated in detail with a combination of steady-state absorption and fluorescence spectroscopy, time-resolved fluorescence, and transient absorption spectroscopy coupled with the aid of computational predictions. Vertical excitation calculations and Franck–Condon simulations allowed for detailed assignment of a multitude of electronic transitions observed in absorption spectroscopy, and assignment of the Franck–Condon active modes contributing to the extensive vibronic activity in the S_0–S_1 region of ADT/2ADT. These analyses allow for an extended evaluation of TA spectral features and vibrational coherences, otherwise unassignable due to the size and complexity of the ADT chromophore. As indicated by calculations, two conformers were observed and isolated for 2ADT *via* fluorescence spectroscopy yielding clear spectroscopic characteristics of a minor *trans* conformer, and dominant cofacial *cis* conformer. The existence of both conformers at room temperature can be rationalized by considering the contributions to the free energy of each structure.

The two conformers exhibit distinct spectral characteristics and excited state dynamics, with the non-interacting *trans* conformer appearing monomer-like, and *cis*-2ADT revealing significant perturbations to both spectroscopy and dynamics due to the interaction between the ADT cores. Time-resolved spectroscopy enabled analysis of the deactivation mechanism of both conformers showing that *trans*-2ADT decays predominantly through fluorescence, while *cis*-2ADT undergoes relaxation into an excimer geometry following excitation, and then decays primarily through internal conversion to the ground state. These results demonstrate the influence of the conformational landscape on the photophysics of covalently-linked dimers, in this case resulting in conformer-specific excited state dynamics.

Time-resolved fluorescence and transient absorption spectroscopy revealed the formation of an excimer structure in *cis*-2ADT, characterized by its emission properties and spectral evolution out of the Franck–Condon S_1 region into the excimer minimum showing a distinct blue-shift of all S_1 ESA features. Comparison of the kinetics for excimer formation in different solvents shows a polarity dependence on the rate, presumed to be related to either stabilization of the excimer geometry or barrier to excimer formation on the excited state surface in polar media, or due to a higher degree of pre-association in the ground state consistent with enhanced excitonic signatures in the 2ADT absorption spectrum in polar solvents. Nevertheless, the decay of the initial S_1 population into the excimer geometry was found to be $\sim$600 ps in acetone and 1.75 ns in toluene, timescales typically long compared to that expected for singlet fission in dimers such as bipentacenes. While the large estimated exothermicity for singlet fission of $\sim$5000–7000 cm^{-1} would suggest that *cis*-2ADT is a prime candidate for singlet fission, assuming adequate electronic coupling, no evidence for singlet fission was found in the current work. Cursory analysis of the excimer state formed in the experiment suggests that its existence should not hinder singlet fission through kinetic competition, nor by energetic arguments as the excimer minimum should still be $>$2000 cm^{-1} above the correlated triplet pair state (*i.e.* retaining exothermicity). Therefore we surmise that the structure of the *cis* conformer yields a negligible coupling matrix element between both the initially populated singlet exciton state and ^{1}(TT), as well as the excimer state and ^{1}(TT). This scenario would reduce the singlet fission rate well below that of excimer formation and the timescale for its relaxation to the ground state; and we note that a predominantly cofacially-stacked structure can lead to both the absence of singlet fission and facile excimer exciton formation, consistent with the present results.

Acknowledgements

The authors gratefully acknowledge the Division of Chemical Sciences, Geosciences, and Biosciences, Office of Basic Energy Sciences of the U.S. Department of Energy through Grant No. DE-SC0015429. SNS thanks the NSF GRFP for funding (grant DGE 11-44155). JEA and RKH thank the U.S. National Science Foundation (grant CMMI-1255494) for support of organic semiconductor synthesis. Triplet sensitization measurements were done using resources of the Center for Functional Nanomaterials, which is a U.S. DOE Office of Science Facility, at Brookhaven National Laboratory under Contract No. DESC0012704.

References

1 M. C. Hanna and A. J. Nozik, *J. Appl. Phys.*, 2006, **100**, 074510.
2 S. Rühle, *Sol. Energy*, 2016, **130**, 139–147.
3 W. Shockley and H. J. Queisser, *J. Appl. Phys.*, 1961, **32**, 510–519.
4 X. T. Feng, A. V. Luzanov and A. I. Krylov, *J. Phys. Chem. Lett.*, 2013, **4**, 3845–3852.
5 M. B. Smith and J. Michl, *Annu. Rev. Phys. Chem.*, 2013, **64**, 361–386.
6 S. R. Yost, J. Lee, M. W. B. Wilson, T. Wu, D. P. McMahon, R. R. Parkhurst, N. J. Thompson, D. N. Congreve, A. Rao, K. Johnson, M. Y. Sfeir, M. G. Bawendi, T. M. Swager, R. H. Friend, M. A. Baldo and T. Van Voorhis, *Nat. Chem.*, 2014, **6**, 492–497.
7 J. C. Johnson, A. J. Nozik and J. Michl, *Acc. Chem. Res.*, 2013, **46**, 1290–1299.
8 M. B. Smith and J. Michl, *Chem. Rev.*, 2010, **110**, 6891–6936.
9 T. C. Berkelbach, M. S. Hybertsen and D. R. Reichman, *J. Chem. Phys.*, 2013, **46**, 1321–1329.
10 R. D. Pensack, A. J. Tilley, S. R. Parkin, T. S. Lee, M. M. Payne, D. Gao, A. A. Jahnke, D. G. Oblinsky, P. F. Li, J. E. Anthony, D. S. Seferos and G. D. Scholes, *J. Am. Chem. Soc.*, 2015, **137**, 6790–6803.
11 G. D. Scholes, *J. Phys. Chem. A*, 2015, **119**, 12699–12705.
12 R. D. Pensack, E. E. Ostroumov, A. J. Tilley, S. Mazza, C. Grieco, K. J. Thorley, J. B. Asbury, D. S. Seferos, J. E. Anthony and G. D. Scholes, *J. Phys. Chem. Lett.*, 2016, **7**, 2370–2375.
13 J. C. Johnson, A. Akdag, M. Zamadar, X. D. Chen, A. F. Schwerin, I. Paci, M. B. Smith, Z. Havlas, J. R. Miller, M. A. Ratner, A. J. Nozik and J. Michl, *J. Phys. Chem. B*, 2013, **117**, 4680–4695.

14 J. N. Schrauben, J. L. Ryerson, J. Michl and J. C. Johnson, *J. Am. Chem. Soc.*, 2014, **136**, 7363–7373.
15 C. C. Gradinaru, J. T. M. Kennis, E. Papagiannakis, I. H. M. van Stokkum, R. J. Cogdell, G. R. Fleming, R. A. Niederman and R. van Grondelle, *Proc. Natl. Acad. Sci. U. S. A.*, 2001, **98**, 2364–2369.
16 S. W. Eaton, S. A. Miller, E. A. Margulies, L. E. Shoer, R. D. Schaller and M. R. Wasielewski, *J. Phys. Chem. A*, 2015, **119**, 4151–4161.
17 E. A. Margulies, C. E. Miller, Y. L. Wu, L. Ma, G. C. Schatz, R. M. Young and M. R. Wasielewski, *Nat. Chem.*, 2016, **8**, 1120–1125.
18 E. Busby, J. L. Xia, Q. Wu, J. Z. Low, R. Song, J. R. Miller, X. Y. Zhu, L. M. Campos and M. Y. Sfeir, *Nat. Mater.*, 2015, **14**, 426–433.
19 C. M. Mauck, P. E. Hartnett, E. A. Margulies, L. Ma, C. E. Miller, G. C. Schatz, T. J. Marks and M. R. Wasielewski, *J. Am. Chem. Soc.*, 2016, **138**, 11749–11761.
20 B. J. Walker, A. J. Musser, D. Beljonne and R. H. Friend, *Nat. Chem.*, 2013, **5**, 1019–1024.
21 M. W. B. Wilson, A. Rao, J. Clark, R. S. S. Kumar, D. Brida, G. Cerullo and R. H. Friend, *J. Am. Chem. Soc.*, 2011, **133**, 11830–11833.
22 S. N. Sanders, E. Kumarasamy, A. B. Pun, M. L. Steigerwald, M. Y. Sfeir and L. M. Campos, *Chem.*, 2016, **1**, 505–511.
23 J. N. Mastron, S. T. Roberts, R. E. McAnally, M. E. Thompson and S. E. Bradforth, *J. Phys. Chem. B*, 2013, **117**, 15519–15526.
24 S. Lukman, A. J. Musser, K. Chen, S. Athanasopoulos, C. K. Yong, Z. B. Zeng, Q. Ye, C. Y. Chi, J. M. Hodgkiss, J. S. Wu, R. H. Friend and N. C. Greenham, *Adv. Funct. Mater.*, 2015, **25**, 5452–5461.
25 J. Zirzlmeier, D. Lehnherr, P. B. Coto, E. T. Chernick, R. Casillas, B. S. Basel, M. Thoss, R. R. Tykwinski and D. M. Guldi, *Proc. Natl. Acad. Sci. U. S. A.*, 2015, **112**, 5325–5330.
26 S. N. Sanders, E. Kumarasamy, A. B. Pun, M. T. Trinh, B. Choi, J. L. Xia, E. J. Taffet, J. Z. Low, J. R. Miller, X. Roy, X. Y. Zhu, M. L. Steigerwald, M. Y. Sfeir and L. M. Campos, *J. Am. Chem. Soc.*, 2015, **137**, 8965–8972.
27 J. E. Anthony, *Chem. Rev.*, 2006, **106**, 5028–5048.
28 S. N. Sanders, E. Kumarasamy, A. B. Pun, K. Appavoo, M. L. Steigerwald, L. M. Campos and M. Y. Sfeir, *J. Am. Chem. Soc.*, 2016, **138**, 7289–7297.
29 S. N. Sanders, E. Kumarasamy, A. B. Pun, M. L. Steigerwald, M. Y. Sfeir and L. M. Campos, *Angew. Chem., Int. Ed.*, 2016, **55**, 3373–3377.
30 N. Korovina, S. Das, Z. Nett, X. Feng, J. Joy, R. Haiges, A. Krylov, S. Bradforth and M. Thompson, *J. Am. Chem. Soc.*, 2016, **138**, 617–627.
31 H. Y. Liu, V. M. Nichols, L. Shen, S. Jahansouz, Y. H. Chen, K. M. Hanson, C. J. Bardeen and X. Y. Li, *Phys. Chem. Chem. Phys.*, 2015, **17**, 6523–6531.
32 H. Saigusa and E. C. Lim, *Acc. Chem. Res.*, 1996, **29**, 171–178.
33 G. D. Scholes, K. P. Ghiggino and G. J. Wilson, *Chem. Phys.*, 1991, **155**, 127–141.
34 F. M. Winnik, *Chem. Rev.*, 1993, **93**, 587–614.
35 M. Pope and C. E. Swenberg, *Electronic Processes in Organic Crystals and Polymers*, Oxford University Press, New York, 2nd edn, 1999.
36 J. G. Laquindanum, H. E. Katz and A. J. Lovinger, *J. Am. Chem. Soc.*, 1998, **120**, 664–672.
37 A. D. Platt, J. Day, S. Subramanian, J. E. Anthony and O. Ostroverkhova, *J. Phys. Chem. C*, 2009, **113**, 14006–14014.
38 Y. D. Zhang, Y. S. Wu, Y. Q. Xu, Q. Wang, K. Liu, J. W. Chen, J. J. Cao, C. F. Zhang, H. B. Fu and H. L. Zhang, *J. Am. Chem. Soc.*, 2016, **138**, 6739–6745.
39 Y. H. Chen, L. Shen and X. Y. Li, *J. Phys. Chem. A*, 2014, **118**, 5700–5708.
40 R. K. Hallani, K. J. Thorley, Y. C. Mei, S. R. Parkin, O. D. Jurchescu and J. E. Anthony, *Adv. Funct. Mater.*, 2016, **26**, 2341–2348.
41 J. J. Snellenburg, S. P. Laptenok, R. Seger, K. M. Mullen and I. H. M. van Stokkum, *J. Stat. Softw.*, 2012, **49**, 1–22.
42 M. J. Frisch, G. W. Trucks, H. B. Schlegel, G. E. Scuseria, M. A. Robb, J. R. Cheeseman, G. Scalmani, V. Barone, B. Mennucci, G. A. Petersson, H. Nakatsuji, M. Caricato, X. Li, H. P. Hratchian, A. F. Izmaylov, J. Bloino, G. Zheng, J. L. Sonnenberg, M. Hada, M. Ehara, K. Toyota, R. Fukuda, J. Hasegawa, M. Ishida, T. Nakajima, Y. Honda, O. Kitao, H. Nakai, T. Vreven, J. Montgomery, J. A. Montgomery, Jr., J. E. Peralta, F. Ogliaro, M. Bearpark, J. J. Heyd, E. Brothers, K. N. Kudin, V. N. Staroverov, R. Kobayashi, J. Normand, K. Raghavachari, A. Rendell, J. C. Burant, S. S. Iyengar, J. Tomasi, M. Cossi, N. Rega, N. J. Millam, M. Klene, J. E. Knox, J. B. Cross, V. Bakken, C. Adamo, J. Jaramillo, R. Gomperts, R. E. Stratmann, O. Yazyev, A. J. Austin, R. Cammi, C. Pomelli, J. W. Ochterski, R. L. Martin, K. Morokuma, V. G. Zakrzewski, G. A. Voth, P. Salvador, J. J. Dannenberg, S. Dapprich, A. D. Daniels, Ö. Farkas, J. B. Foresman, J. V. Ortiz, J. Cioslowski and D. J. Fox, *R. A. Gaussian 09*, Gaussian, Inc., Wallingford, CT, 2009.
43 T. Yanai, D. P. Tew and N. C. Handy, *Chem. Phys. Lett.*, 2004, **393**, 51–57.
44 E. Busby, T. C. Berkelbach, B. Kumar, A. Chernikov, Y. Zhong, H. Hlaing, X. Y. Zhu, T. F. Heinz, M. S. Hybertsen, M. Y. Sfeir, D. R. Reichman, C. Nuckolls and O. Yaffe, *J. Am. Chem. Soc.*, 2014, **136**, 10654–10660.
45 A. A. Bakulin, S. E. Morgan, T. B. Kehoe, M. W. B. Wilson, A. W. Chin, D. Zigmantas, D. Egorova and A. Rao, *Nat. Chem.*, 2016, **8**, 16–23.
46 J. Clark, C. Silva, R. H. Friend and F. C. Spano, *Phys. Rev. Lett.*, 2007, **98**, 206406.
47 F. C. Spano, *Acc. Chem. Res.*, 2010, **43**, 429–439.
48 J. C. Dean, S. Rafiq, D. G. Oblinsky, E. Cassette, C. C. Jumper and G. D. Scholes, *J. Phys. Chem. A*, 2015, **119**, 9098–9108.
49 K. E. Brown, W. A. Salamant, L. E. Shoer, R. M. Young and M. R. Wasielewski, *J. Phys. Chem. Lett.*, 2014, **5**, 2588–2593.
50 J. M. Giaimo, J. V. Lockard, L. E. Sinks, A. M. Scott, T. M. Wilson and M. R. Wasielewski, *J. Phys. Chem. A*, 2008, **112**, 2322–2330.
51 S. R. Long, Y. Y. Wang, S. Vdovic, M. Zhou, L. Y. Yan, Y. L. Niu, Q. J. Guo and A. D. Xia, *Phys. Chem. Chem. Phys.*, 2015, **17**, 18567–18576.
52 N. Reilly, M. Ivanov, B. Uhler, M. Talipov, R. Rathore and S. A. Reid, *J. Phys. Chem. Lett.*, 2016, **7**, 3042–3045.